IEEE Photonics Journal
An IEEE Photonics Society Publication

Open Access

Temporal Imaging of Optical Asymmetric Waveform Pulses With a Time Lens

Volume 7, Number 4, August 2015

Azusa Hasegawa
Ken Kashiwagi
Yosuke Tanaka
Takashi Kurokawa

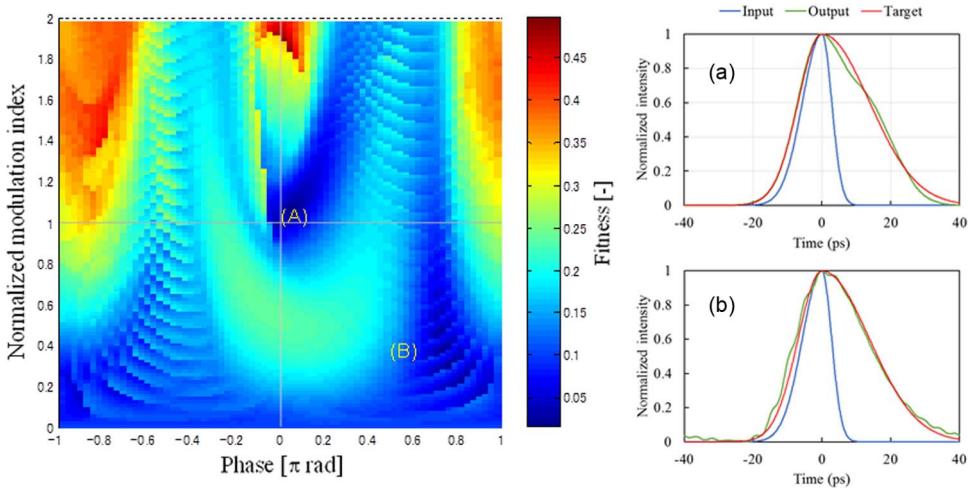

DOI: 10.1109/JPHOT.2015.2464078
1943-0655

IEEE photonics SOCIETY

IEEE

Temporal Imaging of Optical Asymmetric Waveform Pulses With a Time Lens

Azusa Hasegawa,[1] Ken Kashiwagi,[1] Yosuke Tanaka,[1] and Takashi Kurokawa[1,2]

[1]Department of Electronic Engineering, Tokyo University of Agriculture and Technology, Tokyo 184-8588, Japan
[2]National Astronomical Observatory of Japan, Tokyo 181-8588, Japan

DOI: 10.1109/JPHOT.2015.2464078

Manuscript received June 30, 2015; revised July 26, 2015; accepted July 28, 2015. Date of publication August 3, 2015; date of current version August 17, 2015. This work was supported in part by a Grant-in-Aid (No. 26286057) from the Japan Society for the Promotion of Science. Corresponding author: Y. Tanaka (e-mail: tyosuke@cc.tuat.ac.jp).

Abstract: In this paper, we investigated the imaging condition of asymmetric pulses on a temporal imaging (TI) system comprising two optical fibers and a phase modulator. We introduced a fitness function to evaluate the difference between target and output waveforms to quantitatively estimate TI characteristics. We successfully determined the optimal combination of phase modulation index and phase deviation to provide good TI by simulating the fitness function. We generated chirp-free pulses with symmetric and asymmetric waveforms using an in-line waveguide pulse synthesizer, i.e., an optical pulse synthesizer, based on pulse shaping and experimentally confirmed the TI condition in a time lens system. Moreover, TI was achieved not only at a theoretical value of the modulation index satisfying the TI condition but at a much smaller value than the theoretical value for a time-reversal mode as well. Measured waveforms of the experimental output agreed with simulation results. This may be important for practical applications because a TI system requires a much smaller modulation power.

Index Terms: Ultrafast technology, pulse shaping.

1. Introduction

For several years, temporal imaging (TI) has been attracting considerable interest from the viewpoint of space-time duality [1]–[4]. A spatial lens produces a quadratic spatial phase shift around a paraxial region for spatial imaging. Similarly, a device operating as a time lens has to produce a nearly quadratic temporal phase shift for pulses. There have been numerous studies on TI systems constructed by cascading input dispersion, time lens, and output dispersion. Such TI systems allow temporal expansion, compression, or reversal of optical waveforms, same as that done by spatial imaging. For communication applications, optical bit streams (optical packets) encoded at nominal rates can be compressed by a TI system and time division multiplexed into much faster bit streams at a transmitter. At a receiver site, ultrafast bit streams can be time division demultiplexed and stretched to a time scale that is accessible to ordinary high-speed photodiodes. Furthermore, a time lens might be useful for transforming bit rates of a pulse train before and after optical packet switching.

One important issue facing the realization of TI systems is the question of how to implement an ideal time lens. Thus far, two methods of implementing a time lens that provides a nearly

quadratic phase modulation have been investigated. One uses nonlinear optical effects including sum-frequency or difference-frequency generation in a nonlinear crystal [5]–[8], and self-phase modulation, cross-phase modulation, or four-wave mixing in a nonlinear fiber or a silicon waveguide [9]–[11]. Nonlinear optical effects can give an ideal quadratic phase modulation; however, this strongly depends on the incident pulse intensity. Nonlinear parametric processes are especially accompanied by large wavelength shifts that produce some difficulties in system applications, including optical communication networks and communication processing.

The other solution is to apply a sinusoidal phase modulation to pulses using an electro-optic (EO) phase modulator [12]–[15]. In-line waveguide phase modulators match with fibers providing input and output dispersions in fiber-optic systems. Wavelength-preserving operation and easy reconfiguration are suitable for communication applications. The temporal magnification factor can be varied easily by selecting the type (normal or anomalous dispersion in a certain wavelength) and length of a fiber. However, in an EO phase modulator, there remain several problems such as deviation from a parabolic profile in a sinusoidal phase modulation, limitation of a phase modulation index achievable by the maximum radio-frequency (RF) power of a modulator, and the tolerance of synchronization between input pulses and modulation signals. Moreover, input pulse width was limited to around 15% of the signal period when a simple sinusoidal voltage was applied to a modulator. The deviation from a parabolic profile (or temporal aberration) degrades the performance of a TI system [16], [17]. Recently, it has been reported that three harmonics of clock frequency can achieve truly parabolic modulation over a time window across 70% of the period [15].

Phase modulation index is limited by the sinusoidal signal power applied to a modulator. In particular, the RF signal power limits the size of the reduction ratio of a pulse waveform because a higher waveform reduction increases the required modulation index. When an input pulse has a symmetric waveform similar to a Gaussian profile, it is clearly realized that the pulse and modulation signal should be synchronized such that the tops of both waveforms coincide with one another. However, the matter of how a modulation signal should be synchronized with an input pulse with an asymmetric waveform similar to that of an optical packet has not been investigated [5], [18], [19].

In this study, we investigated the imaging condition of asymmetric pulses on a TI system comprising two optical fibers and a phase modulator. It is important to clarify the imaging condition of asymmetric pulses because they are used to confirm the temporal reversal and are used as optical packets in practical applications. We introduced a fitness function to evaluate the difference between target and output waveforms in a TI system to quantitatively estimate TI characteristics. We successfully determined the optimal combination of phase modulation index and phase deviation to provide good TI by simulating the fitness function. Experimentally, it is critical to prepare a chirp-free pulse with an asymmetric waveform as an input pulse. Our developed optical-pulse-shaping technology enables the generation of picosecond pulses with asymmetric waveforms. We generated symmetric and asymmetric pulses using an in-line waveguide pulse synthesizer, i.e., optical pulse synthesizer (OPS), based on pulse shaping [20]–[22] and experimentally confirmed the TI condition in a time lens system. Measured waveforms of the experimental output agree with simulation results.

2. Simulation

A typical TI system for optical pulses is constructed by cascading input dispersion, quadratic phase modulation, and output dispersion. Fig. 1 shows the schematic of a TI system that we have investigated in this study.

2.1. Theoretical Background for Simulation

A TI system is comprised of an input optical fiber with group-velocity dispersion D_{in} in units of ps/nm, a waveguide phase modulator, and an output fiber with group-velocity dispersion D_{out}. When the repetition frequency of a pulse train incident on a time lens is ν_m, the sinusoidal modulation

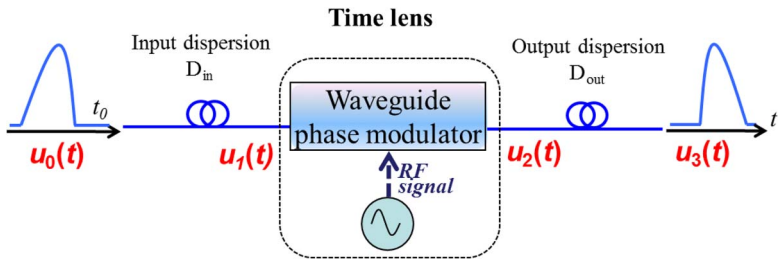

Fig. 1. Schematic of a TI system comprising two optical fibers and a phase modulator driven by a sinusoidal RF signal.

signal given to a phase modulator must have the same frequency to be synchronized. The phase shift induced by the modulator can be described as

$$\Gamma(t) = \phi_m \cos(2\pi\nu_m t + \theta) \tag{1}$$

where ϕ_m is the phase modulation index, and θ is the phase deviation between the peak of an input pulse and the top of a modulation signal.

We perform the simulation through the process as follows: a chirp-free pulse, $u_0(t)$, that propagates through an input fiber and a pulse waveform in front of a phase modulator can be written as

$$u_1(t) = \frac{\sqrt{i}}{\lambda_0}\sqrt{\frac{c}{D_{in}}}\int_{-\infty}^{\infty} u_0(t_0)\exp\left[-i\frac{\pi c}{\lambda_0^2 D_{in}}(t-t_0)^2\right]dt_0 \tag{2}$$

where λ_0 is the carrier wavelength of an optical pulse, and a constant phase change due to the propagation in the fiber is omitted. After modulation, the pulse waveform $u_2(t)$ can be written as

$$u_2(t) = u_1(t)\exp[-i\phi_m \cos(2\pi\nu_m t + \theta)]. \tag{3}$$

Finally, after propagating through an output fiber, the pulse waveform $u_3(t)$ is written as

$$u_3(t) = \frac{\sqrt{i}}{\lambda_0}\sqrt{\frac{c}{D_{\text{out}}}}\int_{-\infty}^{\infty} u_2(t_1)\exp\left[-i\frac{\pi c}{\lambda_0^2 D_{\text{out}}}(t-t_1)^2\right]dt_1. \tag{4}$$

If an input optical pulse is sufficiently shorter than the repetition period of a modulation signal, the phase modulation can be considered to be quadratic and described by

$$u_2(t) \cong u_1(t)\exp\left[i2\pi^2\phi_m\nu_m^2(\cos\theta)t^2\right] \tag{5}$$

by omitting the constant phase change. On the contrary, when we define an ideal quadratic phase modulation characterized by a focal time given by

$$f_t \equiv \frac{c}{2\pi\lambda_0^2\phi_m\nu_m^2(\cos\theta)}. \tag{6}$$

Equation (5) can be rewritten as follows:

$$u_2(t) \cong u_1(t)\exp\left[\frac{i\pi c t^2}{\lambda_0^2 f_t}\right]. \tag{7}$$

If we define a temporal magnification factor M as

$$M = -D_{\text{out}}/D_{\text{in}} \tag{8}$$

the output pulse waveform $u_3(t)$ can be written as

$$u_3(t) = \frac{1}{\sqrt{M}} \exp\left\{\frac{i\pi c}{\lambda_0^2 f_t M} t^2\right\} u_0\left(\frac{t}{M}\right) \tag{9}$$

when the belowmentioned ideal TI condition is satisfied

$$1/D_{\text{in}} + 1/D_{\text{out}} = \frac{1}{f_t}. \tag{10}$$

Equation (9) suggests that an output waveform emerges temporally rescaled according to the magnification factor after passing through the TI system. The output waveform would be magnified for $|M| > 1$, whereas it would be reduced for $|M| < 1$. Furthermore, the output waveform is time reversed from the input one when M is negative.

When the TI condition is satisfied, the focal time is written on the basis of (8) and (10) as

$$f_t = \frac{M}{M-1} D_{\text{in}}. \tag{11}$$

If we set D_{in} to be positive, the value of the focal time is positive and $|\theta| < \pi/2$ according to (11) when $M > 1$ or $M < 0$. On the other hand, the f_t value must be negative and $\pi/2 < |\theta| < \pi$ when $0 < M < 1$.

The value of the phase modulation index required to satisfy the TI condition is theoretically obtained from the (6) and (11) as

$$\phi_m = \frac{M-1}{M} \cdot \frac{c}{2\pi\lambda_0^2 \nu_m^2 D_{\text{in}} \cos\theta}. \tag{12}$$

Then, the standard value of the required phase modulation index is defined as

$$\phi_m^s \equiv \left|\frac{M-1}{M}\right| \frac{c}{2\pi\lambda_0^2 \nu_m^2 D_{\text{in}}}. \tag{13}$$

In actual experiments, a phase modulation index is limited by a sinusoidal signal power input into a phase modulator. As the input impedance of a modulator is 50 Ω, the phase modulation index depends on a modulation signal power input into a phase modulator as follows:

$$\phi_m = 10\pi\sqrt{P}/V_\pi \tag{14}$$

where P is the average power of a modulation signal, and V_π is the half-wave voltage of a phase modulator. The typical characteristic of the phase modulator that we use is $V_\pi =$ 4 V at 12.5 GHz and the maximum modulation signal power is 4 W. Thus, the maximum phase modulation index is calculated to be 5π rad. As a result, the magnification factor and input dispersion must be set under the condition that the value of the phase modulation index calculated from (13) does not exceed 5π rad.

According to (13), it appears that the increment of input dispersion may make the required modulation index smaller; however, the input pulse would be broadened such that it does not maintain a parabolic modulation if input dispersion was increased. When the Gaussian pulse with a width of T_i propagates through an input fiber with dispersion D_{in}, the broadened pulse width, T_i', is roughly approximated as follows:

$$T_i' \cong 2\ln 2 \times \frac{\lambda_0^2 D_{\text{in}}}{\pi c T_i}. \tag{15}$$

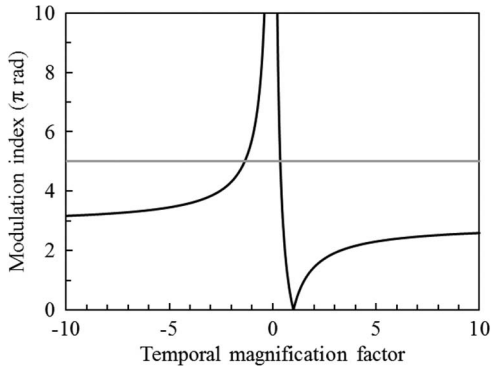

Fig. 2. Relation between the magnification factor and standard value of the required phase modulation index for TI when $\lambda_0 = 1553$ nm, $\nu_m = 12.5$ GHz, and $D_{\text{in}} = 14$ ps/nm.

Because the broadened pulse width T_i' should be less than approximately 15% of the signal period, the input dispersion value must satisfy the condition as follows:

$$D_{\text{in}} < \frac{\pi c T_i}{(16\ln 2)\lambda_0^2 \nu_m}. \tag{16}$$

We perform simulation and experiments under the condition that the input pulse width is 10 ps, central wavelength of the input pulse is 1553 nm, and pulse repletion frequency is 12.5 GHz. Input dispersion is set to be 14 ps/nm based on (16). The standard value of the required phase modulation index dependence on the magnification factor is calculated as shown in Fig. 2. It can be seen that a small waveform reduction around zero becomes difficult as the required modulation index exceeds 5π rad.

Output pulse width from the TI system is $|M|T_i$. Because it should be less than a time window, the magnification factor must satisfy the condition as follows:

$$|M| < \frac{T_m}{2T_i}. \tag{17}$$

Because the pulse width was set to be 10 ps in our experiments, the magnification factor was limited to the range of $|M| < 4$ based on (17).

2.2. Simulation Results

Actual TI characteristics must be analyzed exclusively by simulation because a time lens cannot produce a perfect parabolic modulation. We calculate the output pulse intensity waveform $|u_3(t)|^2$ according to (2)–(4) by varying both the phase modulation index and phase deviation. To determine the combination of (ϕ_m, θ) that provides good TI, we introduce a fitness function defined as the difference between the calculated output waveform and target waveform enlarged or reduced from an input waveform with a certain magnification factor. The fitness function is defined as

$$\text{fitness} = \frac{\sum |p(t_i) - o(t_i)|}{N} \tag{18}$$

where $p(t_i)$ and $o(t_i)$ are the values of target and output waveforms, respectively, at the sampling point t_i, and N is the total number of sampling points.

Input dispersion is set to be $+14$ ps/nm and output dispersion is set according to the magnification factor; the same parameters are used in the experiments described in the next section. The input pulse has a 12.5-GHz repetition rate and a symmetric or an asymmetric Gaussian

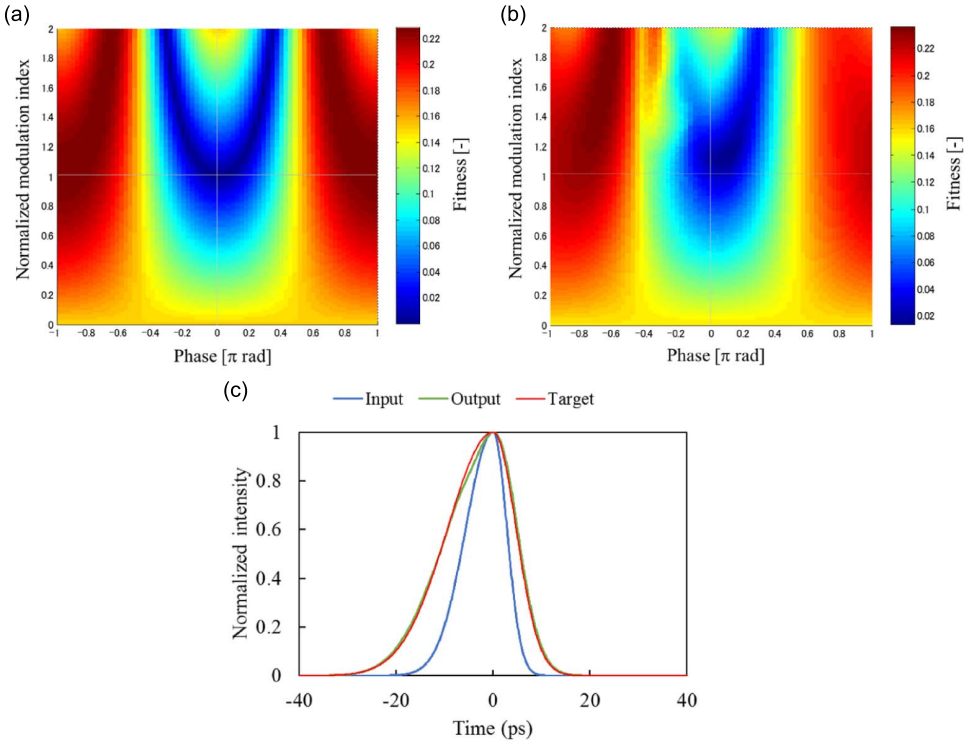

Fig. 3. Simulation results for the temporal magnification of the pulse waveform when $M = +1.66$ ($D_{\text{in}} = +14.0$ ps/nm and $D_{\text{out}} = -23.2$ ps/nm). Fitness maps for (a) symmetric input pulse and (b) asymmetric input pulse. Vertical axes in both (a) and (b) are normalized by the standard value of the modulation index, which is calculated to be 1.14π. (c) The calculated output waveform for the asymmetric input waveform at the best-fitting point ($\theta = 0.07\pi$ and $\phi_m = 1.30\pi$). Blue, green, and red curves indicate input, output, and target waveforms, respectively.

waveform with a FWHM of 10 ps. The asymmetric waveform comprises two half-Gaussian waveforms with HWHMs of 6.7 ps and 3.3 ps, whose ratio is 2 : 1.

The first case is the time-unreversed magnification of a pulse waveform $(M > 1)$. We calculate fitness functions for both symmetric and asymmetric pulses when $M = +1.66$ ($D_{\text{in}} = +14.0$ ps/nm and $D_{\text{out}} = -23.2$ ps/nm). The calculated results are shown in Fig. 3(a) for the symmetric pulse and in (b) for the asymmetric pulse. The fitness function is plotted by the phase deviation on the horizontal axis and the modulation index normalized with the standard value $(= 1.14\pi)$ calculated from (13) on the vertical axis. The function is represented on a two-dimensional map, where the fitness level is shown as a color bar ranging from blue (best fitness) to red (worst fitness).

The fitness map for the symmetric pulse exhibits symmetry across the vertical axis, as shown in Fig. 3(a), and the best fitness is obtained when the phase deviation is 0 and the normalized modulation index is 1, as shown in Fig. 3(a). On the other hand, the fitness map for the asymmetric pulse does not exhibit symmetry and the best-fitting point is offset slightly from the center to upper right, as shown in Fig. 3(b). The output waveform calculated at the best-fitting point for the asymmetric pulse agrees well with the target waveform, as shown in Fig. 3(c). Note that a small phase deviation and a slight increase of the modulation index provide the best TI condition for the asymmetric pulse. The small phase deviation, in fact, induces the slight increase of the modulation index, which is consistent with (12).

The second case is the time-unreversed reduction of a pulse waveform $(0 < M < 1)$. We calculate fitness functions for asymmetric pulses when $M = +0.5$ ($D_{\text{in}} = +14.0$ ps/nm and $D_{\text{out}} = -7.0$ ps/nm) because the required modulation index exceeds the RF power limit abruptly as the magnification factor approaches zero. Fig. 4(a) shows the fitness map, which does not

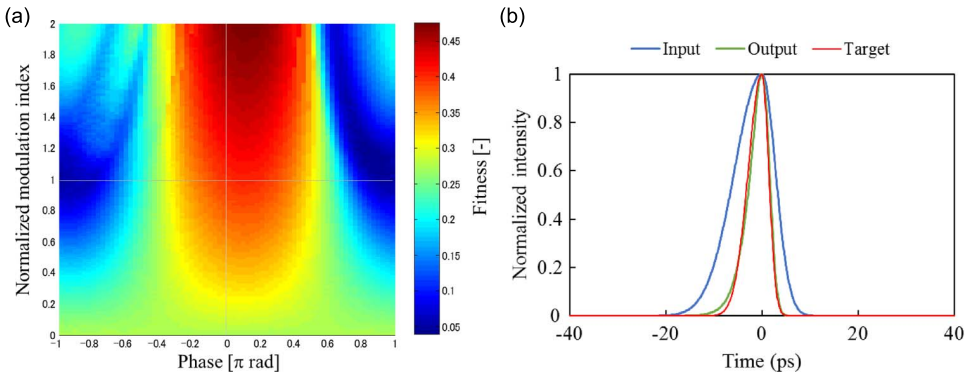

Fig. 4. Simulated results for the temporal reduction of a pulse waveform when $M = +0.5$ ($D_{\text{in}} = +14.0$ ps/nm and $D_{\text{out}} = -7.0$ ps/nm). (a) Fitness map for the asymmetric input pulse with a FWHM of 10 ps. The vertical axis is normalized by the standard value of the modulation index 2.88π. (b) Calculated output waveform at the best-fitting point ($\theta = 0.90\pi$ and $\phi_m = 3.03\pi$).

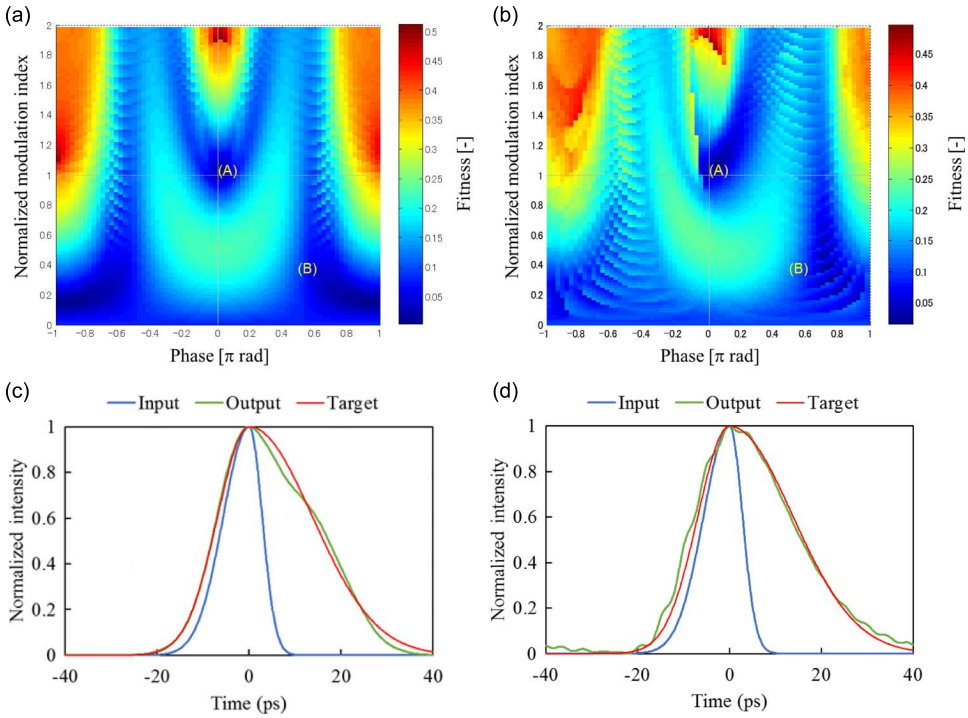

Fig. 5. Simulated results for a time-reversed magnification of a pulse waveform when $M = -2.43$ ($D_{\text{in}} = +14.0$ ps/nm and $D_{\text{out}} = +34.0$ ps/nm). Fitness maps for (a) symmetric pulse and (b) asymmetric pulse. Vertical axes in both maps are normalized by the standard value of the modulation index, 4.07π. For asymmetric pulses, the calculated output waveforms at the points A ($\theta = 0.028\pi$ and $\phi_m = 4.27\pi$) and B ($\theta = 0.78\pi$ and $\phi_m = 1.32\pi$) in (b) are shown in (c) and (d), respectively.

exhibit symmetry across the vertical axis. The best-fitting points are distributed around the region where the phase deviation is close to π and the normalized modulation index is slightly larger than 1. The calculated output waveform at the best-fitness point ($\theta = 0.90\pi$ and $\phi_m = 3.03\pi$) agrees well with the target waveform, as shown in Fig. 4(b).

The last case is that of the time reversal of a pulse waveform $(M < 0)$. We calculate the fitness functions for both symmetric and asymmetric pulses when $M = -2.43$ ($D_{\text{in}} = +14.0$ ps/nm and $D_{\text{out}} = +34.0$ ps/nm). Fitness maps for symmetric and asymmetric pulses are shown in

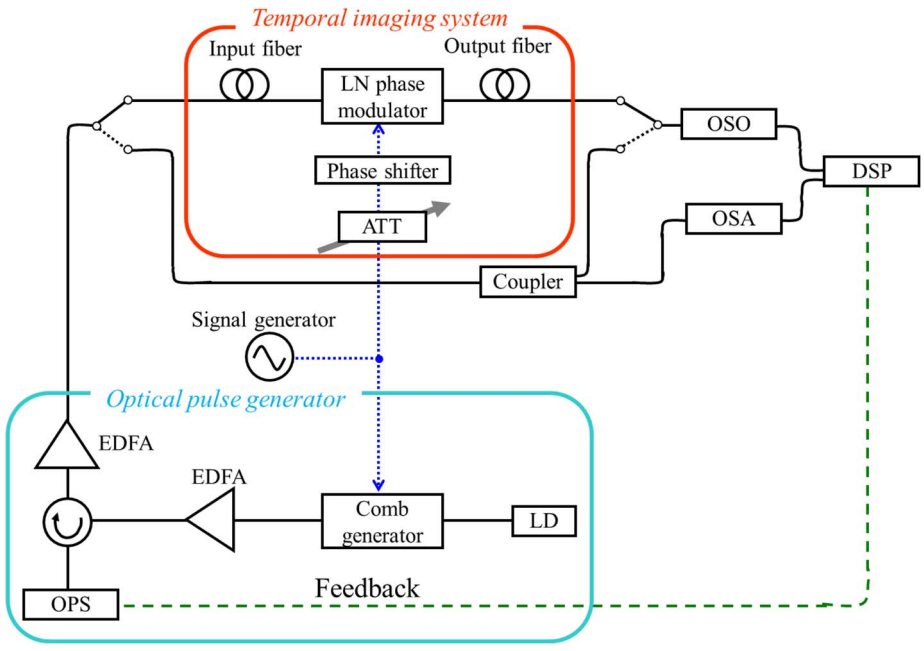

Fig. 6. Experimental setup consisting of a TI system, an optical pulse generator, and an observation site.

Figs. 5(a) and (b), respectively. The standard value of the modulation index is calculated to be 4.07π, which is significantly larger than that in the case of time non-reversal. The fitness map for the symmetric pulse exhibits symmetry across the vertical axis, as shown in Fig. 5(a), and the best-fitting points are distributed around the center of the map. On the other hand, the fitness map for the asymmetric pulse does not exhibit symmetry, and the best-fitting points are offset slightly from the center to upper right, as shown in Fig. 5(b). These characteristics are almost identical to those in the case of time non-reversal, as shown in Fig. 3.

As shown in Figs. 3 and 5, fitness distribution in the case of time reversal has another tendency differing from that of time non-reversal, i.e., the best-fitting points are distributed not only at the center area but also in lower areas with smaller modulation indices. For the symmetric pulse, the best sampling points are distributed in the lower right and lower left areas but not at the center area in symmetry. On the other hand, for the asymmetric pulse, the best sampling points are distributed in lower right areas but not at the center area. The calculated output waveforms at points A and B for the asymmetric pulse agree well with the target waveforms, as shown in Fig. 5(c) and (d), respectively. Note that even a much smaller modulation index can provide good TI because it allows a phase modulator to be driven by much smaller modulation voltages. As a result of the fitness calculation for various M values, it is found that the best sampling-point area other than the center emerges on the map only for the time-reversal case, including waveform reduction, although it disappears with the increase of $|M|$.

3. Experiments

Fig. 6 shows an experimental setup consisting of a TI system, an optical pulse generator, and an observation site. The TI system comprises input and output fibers as dispersive media; these fibers are connected to the in and out of the phase modulator, respectively. A standard single-mode fiber with a dispersion of 14 ps/nm (at 1550 nm) is used as the input fiber. We prepare two types of output fibers according to the two experiments. A normal-dispersion fiber with a dispersion of -23.2 ps/nm (at 1,550 nm) is used as the output fiber in the experiments for time-unreversed magnification $(M = +1.66)$. A standard single-mode fiber with a dispersion of

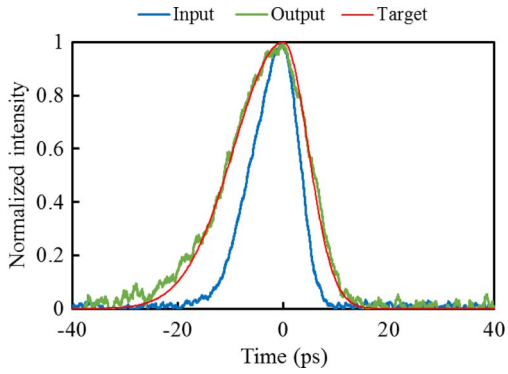

Fig. 7. Observed input and output waveforms compared with the target waveform from the TI system with a magnification factor of $+1.66$ and a modulation index of 1.2π.

34 ps/nm (at 1,550 nm) is used as the output fiber in the experiments with time-reversed magnification $(M = -2.43)$. A sinusoidal modulation signal is given to the phase modulator through a phase shifter that controls the phase deviation between the input pulse and modulation signal.

The optical pulse generator for input pulses to the TI system mainly comprises a laser diode, a comb generator, and an OPS. Two LN phase modulators that are driven by RF signals of 12.5 GHz and 25.0 GHz produce 30 sidebands with 12.5-GHz spacing around CW light $(\lambda = 1552.63$ nm$)$ from the LD. This light is amplified and subsequently input to the OPS. The OPS contains an arrayed waveguide grating to separate each frequency components into 30 channel waveguides with 12.5-GHz spacing. Each frequency component is independently manipulated by the intensity and phase modulators installed in each of the channel waveguides. They are integrated on a single chip fabricated by silica-based planar waveguide technology. The target spectrum is obtained by the Fourier transform of an input pulse waveform. The power spectrum is adjusted to its target form using the OPS by observing the output power spectrum with an optical spectrum analyzer. Then, the phase spectrum is adjusted to obtain the target waveform by measuring the time trace with an optical sampling oscilloscope (bandwidth $\geq$ 500 GHz, time resolution $\sim$1.2 ps). The phase spectrum is adjusted by a genetic-algorithm-based feedback control of the phase modulators such that the differences between the target and measured waveforms are minimized [23]. We generate chirp-free symmetric and asymmetric Gaussian pulses with a width of 10 ps. The asymmetric Gaussian pulse comprises two half-Gaussian waveforms with different widths and a ratio of 2:1. The generated pulse waveforms agree well with the target waveforms.

4. Experimental Results and Discussion

Fig. 7 shows the experimental result for the time-unreversed magnification, in which a 10-ps-wide asymmetric Gaussian pulse is input into the TI system with a magnification factor of $+1.66$. The power and the phase of the RF modulation signal applied to the phase modulator are controlled by an RF attenuator and the phase shifter to agree with the target waveform. Blue, green, and red curves indicate input, output, and target waveforms, respectively. Output and target waveforms match most closely when the modulation index is set to be 1.2π which is slightly larger than its standard value. Thus, it is difficult to measure the phase shift. The increase of the magnification factor over 3.5 degrades the output waveform because it is very large to fit in the time window.

Fig. 8 shows the experimental result for the time-reversed magnification in the case where a 10-ps-wide asymmetric Gaussian pulse is input into the TI system with a magnification factor of -2.43. Output and target waveforms match most closely at the center best-fitting area when the modulation index is set to 4.3π. On the contrary, a temporally imaged output is observed in the lower right area of the fitness map where the modulation index is set to be a much smaller value 1.29π, as shown in Fig. 8(b). The observed waveform agrees with the target waveform, although there is a little noise because of the poor input power to the sampling oscilloscope.

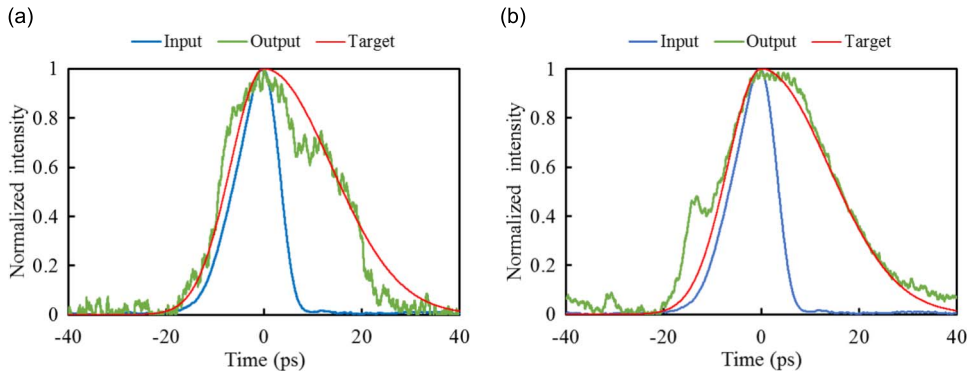

Fig. 8. Observed input and output waveforms compared with the target waveform from the TI system with a magnification factor of -2.43 and a modulation index of (a) 4.3π and (b) 1.29π.

Here, let us examine why good TI can be obtained even in a very small modulation index region only in the case of time reversal. The standard value of the modulation index for a magnification factor of -2.43 is 4.07π, whereas that for a magnification factor of $+2.43$ is calculated to be 1.68π, which is much smaller than 4.07π. According to the simulation, the output waveform should be time-reversed when the phase deviation from zero goes to π even with a positive magnification factor of $+2.43$. This suggests that TI with a much smaller modulation index corresponds to the case with a magnification factor of $+2.43$ with a large phase deviation.

The theoretical modulation index required for time-reversed imaging $(M < 0)$ is much larger than that for time-unreversed imaging $(M > 0)$ because the modulation index is proportional to $|(M-1)/M|$. The difference between the two modulation index values required for $M > 0$ and $M < 0$ is reduced as $|M|$ increases. As a result of the fitness calculation for various M values, it is found that the best sampling-point area other than the center area emerges on the map for the time reversal case, including waveform reduction, although it disappears with the increase of $|M|$.

Finally, we discuss the influence of the deviation from a parabolic profile in a sinusoidal phase modulation. In our time lens system, the time range that the parabolic approximation holds is 20 ps in the period of 80 ps. The simulation results suggest that asymmetric input pulses with FWHMs of 7–11 ps provide time-reversed TI with a magnification factor of -2.43 for an input dispersion of 14 ps/nm. However, the TI is not perfect as shown in Fig. 5(c) and (d). A little difference between the simulated output waveform and target waveform is due to the deviation from the parabolic profile in a sinusoidal phase modulation. In fact, the simulation using the parabolic phase modulation shows a perfect accordance between the output waveform and target waveform. As the phase modulation index becomes smaller, the influence of the deviation from the parabolic phase modulation becomes smaller for the same input dispersion and the same pulse width. Actually, in the case of time-unreversed magnification with a smaller modulation index, the output waveform agrees well with the target waveform as shown in Fig. 3(c). Using both fundamental and high-order harmonic signals for driving a phase modulator would approach a parabolic phase modulation and enlarge the duration of input pulses.

5. Summary

We investigated a TI system that comprises two optical fibers and a phase modulator. In particular, we investigated the TI condition for input pulses with asymmetric waveforms. By introducing a fitness function to evaluate the difference between target and output waveforms, we quantitatively simulated the effect of a phase modulation index and phase deviation on TI.

We generated chirp-free pulses with symmetric and asymmetric waveforms using an in-line waveguide pulse synthesizer based on pulse shaping and experimentally confirmed the TI condition. As a result, we found eminent and novel features for TI. First, we successfully determined the optimal combination of the phase modulation index and phase deviation to provide good TI

by simulating the fitness function. Second, a small phase deviation was found to provide the best TI condition for the asymmetric waveform. Finally, TI was achieved not only at the theoretical value of the modulation index satisfying the TI condition but also at a much smaller value of the time-reversal mode. Measured waveforms of the experimental output agreed with simulation results. This may be important for practical applications because the TI system requires much less modulation power.

References

[1] E. B. Treacy, "Optical pulse compression with diffraction gratings," *IEEE J. Quantum Electron.*, vol. 5, no. 9, pp. 454–458, Sep. 1969.
[2] T. Jannson and J. Jannson, "Temporal self-imaging effect in single-mode fibers," *J. Opt. Soc. Amer.*, vol. 71, no. 11, pp. 1373–1376, Nov. 1981.
[3] B. H. Kolner and M. Nazarathy, "Temporal imaging with a time lens," *Opt. Lett.*, vol. 14, no. 12, pp. 630–632, Jun. 1989.
[4] B. H. Kolner, "Space-time duality and the theory of temporal imaging," *IEEE J. Quantum Electron.*, vol. 30, no. 8, pp. 1951–1963, Aug. 1994.
[5] C. V. Bennett, R. P. Scott, and B. H. Kolner, "Temporal magnification and reversal of 100 Gb/s optical data with an up-conversion time microscope," *Appl. Phys. Lett.*, vol. 65, no. 20, pp. 2513–2515, Nov. 1994.
[6] C. V. Bennett and B. H. Kolner, "Upconversion time microscope demonstrating 103 $\times$ magnification of femtosecond waveforms," *Opt. Lett.*, vol. 24, no. 11, pp. 783–785, Jun. 1999.
[7] C. V. Bennett and B. H. Kolner, "Principles of parametric temporal imaging—Part 1: System configurations," *IEEE J. Quantum Electron.*, vol. 36, no. 4, pp. 430–437, Apr. 2000.
[8] C. V. Bennett and B. H. Kolner, "Principles of parametric temporal imaging—Part 2: System performance," *IEEE J. Quantum Electron.*, vol. 36, no. 6, pp. 649–655, Jun. 2000.
[9] L. K. H. Mouradian, F. Louradour, V. Messager, A. Barthelemy, and C. Froehly, "Spectro-temporal imaging of femtosecond events," *IEEE J. Quantum Electron.*, vol. 36, no. 7, pp. 795–801, Jul. 2000.
[10] T. T. Ng *et al.,* "Compensation of linear distortions by using XPM with parabolic pulses as a time lens," *IEEE Photon. Technol. Lett.*, vol. 20, no. 13, pp. 1097–1099, Jul. 2008.
[11] R. Salem *et al.,* "Optical time lens based on four-wave mixing on a silicon chip," *Opt. Lett.*, vol. 33, no. 10, pp. 1047–1049, May 2008.
[12] A. A. Godil, B. A. Auld, and D. M. Bloom, "Time-lens producing 1.9 ps optical pulses," *Appl. Phys. Lett.*, vol. 62, no. 10, pp. 1047–1049, Mar. 1993.
[13] A. A. Godil, B. A. Auld, and D. M. Bloom, "Picosecond time-lenses," *IEEE J. Quantum Electron.*, vol. 30, no. 3, pp. 827–837, Mar. 1994.
[14] J. van Howe and C. Xu, "Ultrafast optical signal processing based upon space-time dualities," *J. Lightw. Technol.*, vol. 24, no. 7, pp. 2649–2662, Jul. 2006.
[15] L. E. Munioz-Camuniez, J. Lancis, J. Ojeda-Castañeda, and P. Andrés, "Electro-optic time lens with an extended time aperture," *J. Opt. Soc. Amer. B*, vol. 27, no. 10, pp. 2110–2115, Oct. 2010.
[16] C. V. Bennett and B. H. Kolner, "Aberrations in temporal imaging," *IEEE J. Quantum Electron.*, vol. 37, no. 1, pp. 20–32, Jan. 2001.
[17] Y. Zhu, J. Kim, and D. J. Gauthier, "Aberration-corrected quantum temporal imaging system," *Phys. Rev. A*, vol. 87, no. 4, Apr. 2013, Art. ID. 043808.
[18] J. Azana, N. K. Berger, B. Levit, and B. Fischer, "Simplified temporal imaging system for optical waveforms," *IEEE Photon. Technol. Lett.*, vol. 17, no. 1, pp. 94–96, Jan. 2005.
[19] M. A. Foster *et al.,* "Ultrafast waveform compression using a time-domain telescope," *Nature Photon.*, vol. 3, no. 10, pp. 581–585, Oct. 2009.
[20] T. Kurokawa *et al.,* "Time-space-conversion optical signal processing using arrayed-waveguide grating," *Electron. Lett.*, vol. 33, no. 22, pp. 1890–1891, Oct. 1997.
[21] K. Mandai *et al.,* "Repetition rate and center wavelength-tunable optical pulse generation using an optical comb generator and a high-resolution arrayed-waveguide grating," *IEEE Photon. Technol. Lett.*, vol. 18, no. 5, pp. 679–681, Mar. 2006.
[22] H. Tsuda, Y. Tanaka, T. Shioda, and T. Kurokawa, "Analog and digital optical pulse synthesizers using arrayed-waveguide gratings for high-speed optical signal processing," *J. Lightw. Technol.*, vol. 26, no. 6, pp. 670–677, Mar. 2008.
[23] Y. Tanaka, R. Kobe, T. Shioda, H. Tsuda, and T. Kurokawa, "Generation of 100-Gb/s packets having 8-Bit return-to-zero patterns using an optical pulse synthesizer with a lookup table," *IEEE Photon. Technol. Lett.*, vol. 21, no. 1, pp. 39–41, Jan. 2009.